REPORT 1082

METHOD OF ANALYSIS FOR COMPRESSIBLE FLOW THROUGH MIXED-FLOW CENTRIFUGAL IMPELLERS OF ARBITRARY DESIGN [1]

By Joseph T. Hamrick, Ambrose Ginsburg, and Walter M. Osborn

SUMMARY

A method is presented for analysis of the compressible flow between the hub and the shroud of mixed-flow impellers of arbitrary design. Axial symmetry was assumed, but the forces in the meridional (hub to shroud) plane, which are derived from tangential pressure gradients, were taken into account.

The method was applied to an experimental mixed-flow impeller. The analysis of the flow in the meridional plane of the impeller showed that the rotational forces, the blade curvature, and the hub-shroud profile can introduce severe velocity gradients along the hub and the shroud surfaces. Choked flow at the impeller inlet as determined by the analysis was verified by experimental results.

INTRODUCTION

Because of the complexity of the numerical solution for a three-dimensional analysis of flow through a centrifugal compressor, most treatments of the problem have been concerned with a two-dimensional analysis of the flow between the pressure side of one impeller blade and the suction side of the preceding blade. Relaxation methods in which it was assumed that no velocity variation existed between the hub and the shroud have been used (reference 1) to give an analysis of the flow between blades. In the conventional mixed-flow centrifugal impeller, however, the nonsymmetrical hub-shroud profile, the nonuniform energy addition across the passage, and the blade-angle variation due to close adherence to radial blade elements may introduce velocity gradients between the hub and the shroud comparable with those between the blades. For mixed-flow compressors, therefore, an analysis of the flow in the meridional plane is required. (The meridional plane is one that passes through and is parallel to the axis of rotation.)

In order to investigate the isentropic compressible flow in the meridional plane, a flow equation based on equilibrium, continuity, and general energy considerations was derived at the NACA Lewis laboratory during 1949–50 and is presented herein. Axial symmetry was assumed, but the forces that result from tangential pressure gradients were taken into account. The numerical solution involves the adaptation of stream-filament theory and the numerical integration of all equations.

The applicability of the method for predicting the flow within the impeller was investigated by analyzing the flow through a mixed-flow centrifugal impeller for which experimental data are available (reference 2). Flow streamlines, pressure distributions, and velocity distributions relative to the impeller for a given set of operating conditions are presented. Theoretical shroud pressures and theoretical maximum weight flows over a range of speeds are compared with those experimentally obtained.

ANALYSIS

An analysis is made in the meridional plane of the mixed-flow impeller. Axial symmetry is assumed, but forces in the meridional plane that are derived from tangential pressure gradients are taken into account. By the use of the methods presented in this analysis, the isentropic compressible flow in the meridional plane may be obtained and shown in terms of the flow streamlines and the velocity and pressure distributions.

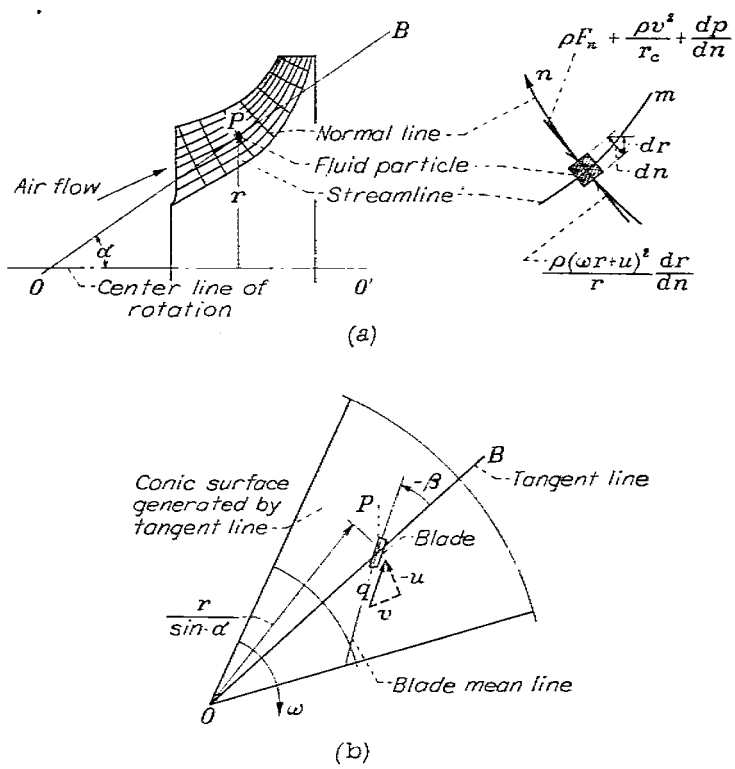

(a) Impeller profile in meridional plane.
(b) Intersection of developed cone surface.

FIGURE 1.—View of impeller showing orientation of blade angle and forces acting on rotating fluid particle in meridional plane.

[1] Supersedes NACA TN 2165, "Method of Analysis for Compressible Flow Through Mixed-Flow Centrifugal Impellers of Arbitrary Design" by Joseph T. Hamrick, Ambrose Ginsburg, and Walter M. Osborn, 1950.

272483—54——34

Geometrical quantities.—A complete geometrical description of the blade is necessary for a numerical solution. Geometrical quantities are defined in appendix A and shown in figures 1 and 2. The blade angle β is oriented in the following manner: In figure 1(a), a line OB, which intersects the axis of rotation at O, is drawn tangent to the point P on a streamline in the meridional plane. If the tangent line OB is rotated about the center line of impeller rotation O–O', a conic surface of revolution that intersects the impeller blades is formed. This intersection is shown on a developed surface of the cone in figure 1(b). At the point of tangency to the streamline (point P), the blade mean line forms the angle $-\beta$ with the tangent line.

Limitations and assumptions.—The fluid is assumed to be nonviscous but compressible. All compression is by the adiabatic, isentropic, steady-flow process. The velocity is assumed uniform from blade to blade in the direction of rotation (axial symmetry) and the average angle of flow relative to the impeller is assumed the same as the blade angle β. This assumption is considered valid where channel flow prevails, but is questionable at the inlet and the outlet.

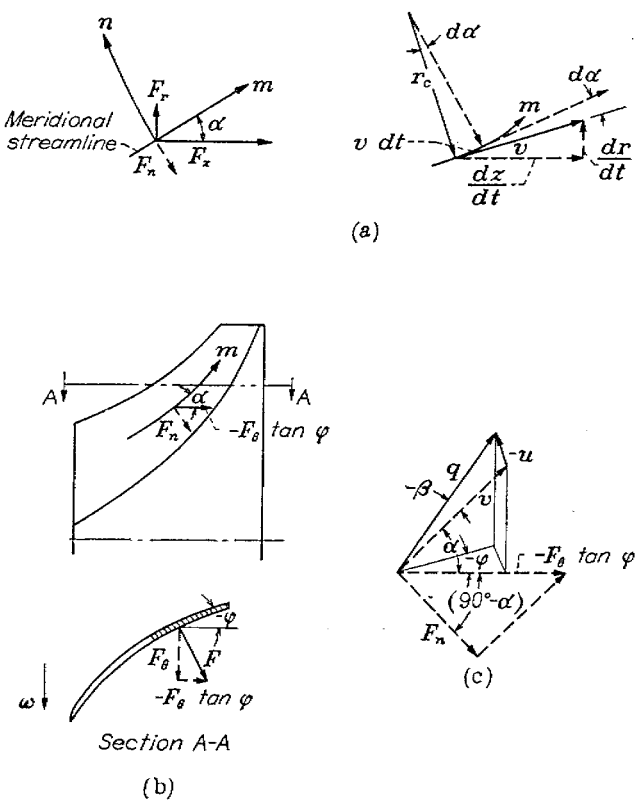

(a) Meridional plane components.
(b) Components of force normal to blade.
(c) Orientation of φ with respect to β. (Dashed lines lie in meridional plane.)

FIGURE 2.—Quantities used in development of force equations.

Method of analysis.—The method is based on one proposed by Flügel for analysis of flow in the blade-to-blade direction and discussed by Stodola in reference 3. The forces acting on a particle along the streamline path are considered. The component of the blade surface force normal to the meridional streamline, the centrifugal forces resulting from the curvilinear path of the particle, and the force due to rotation about the axis of the impeller are equated to the change in pressure across the particle in the hub-to-shroud direction. The resulting force equation is combined with one based on the general energy equation to give an equation involving the relative velocity q and a number of variables dependent upon the geometry of the impeller. The variables that lend themselves to graphical treatment are lumped into two parameters giving a first-order differential equation linear in q. This equation is used in conjunction with the continuity equation to obtain the velocity distribution. Streamlines between the hub and the shroud similar to those shown in figure 1 (a) are drawn in by estimate. When the differential equation is solved for q and a velocity is assumed at the hub, the velocity distribution from hub to shroud may be obtained by numerical integration. By means of the continuity equation, the weight flow corresponding to the assumed hub velocity is obtained. Several solutions may be necessary for obtaining the desired weight flow. The streamlines may be rearranged to match the new values of velocity and density and the complete analysis repeated.

Force equation.—For the forces acting on the fluid particle in the n direction on the meridional plane (fig. 1 (a)), the following equation is obtained (appendix B):

$$\frac{1}{\rho}\frac{dp}{dn}=-\frac{v^2}{r_c}+\frac{(\omega r+u)^2}{r}\frac{dr}{dn}-F_n \tag{1}$$

From figure 1 it can be seen that

$$v=q\cos\beta$$

and

$$u=q\sin\beta$$

In terms of q, equation (1) becomes

$$\frac{1}{\rho}\frac{dp}{dn}=q^2\left(-\frac{\cos^2\beta}{r_c}+\frac{\sin^2\beta}{r}\frac{dr}{dn}\right)+\omega^2 r\frac{dr}{dn}+2\omega q\sin\beta\frac{dr}{dn}-F_n \tag{2}$$

Energy addition.—From general energy considerations, the isentropic adiabatic energy addition is

$$\frac{1}{g}\left[\omega r_1(\omega r_1+u_1)-\omega\lambda_1\right]=h_1\frac{1}{2g}\left[(\omega r_1+u_1)^2+v_1^2\right]-H_t$$

where the prerotation term $\lambda=r_i(\omega r_i+u_i)$

$$h_1-\frac{\omega^2 r_1^2}{2g}+\frac{u_1^2}{2g}+\frac{v_1^2}{2g}=H_t-\frac{\omega\lambda_1}{g} \tag{3}$$

From figure 1,

$$q^2=u^2+v^2$$

and with the assumption that H_t is constant for all streamlines,

$$h_1-\frac{1}{2g}\left[(\omega r_1)^2-q_1^2\right]+\frac{\omega\lambda_1}{g}=h_0-\frac{1}{2g}\left[(\omega r_0)^2-q_0^2\right]+\frac{\omega\lambda_0}{g}$$

$$h_1-h_0=\frac{1}{2g}\left[\omega^2(r_1^2-r_0^2)-(q_1^2-q_0^2)-2\omega(\lambda_1-\lambda_0)\right]$$

For an isentropic process

$$h_1-h_0=\int_0^1 \frac{1}{\rho g}\,dp$$

Therefore

$$\int_0^1 \frac{1}{\rho g}\,dp=\frac{1}{2g}\left[\omega^2(r_1^2-r_0^2)-(q_1^2-q_0^2)-2\omega(\lambda_1-\lambda_0)\right] \tag{4}$$

When differentiated with respect to n, equation (4) becomes

$$\frac{1}{\rho}\frac{dp}{dn}=\omega^2 r\frac{dr}{dn}-q\frac{dq}{dn}-\omega\frac{d\lambda}{dn} \tag{5}$$

General velocity equation.—Equations (2) and (5) are combined to give the following equation:

$$\frac{dq}{dn}=q\left(\frac{\cos^2\beta}{r_c}-\frac{\sin^2\beta}{r}\frac{dr}{dn}\right)-2\omega\sin\beta\frac{dr}{dn}+\frac{F_n}{q}-\frac{\omega}{q}\frac{d\lambda}{dn} \tag{6}$$

For straight blades lying on the meridional plane with no prerotation of the fluid at the inlet, the terms $\frac{F_n}{q}$ and $\frac{\omega}{q}\frac{d\lambda}{dn}$ drop out; a first-order differential equation linear in q thus remains. In order to arrive at a solution for curved-blade impellers and for prerotation at the inlet, it may be desirable to solve for q and to neglect these terms in the first solution. The values of q thus found may be used in the force and prerotation terms for the second solution and may be treated in the same manner as those terms dependent upon the geometry of the impeller.

Velocity equation for impeller of arbitrary blade shape having radial blade elements with no prerotation.—The blade-force component F_n normal to the meridional streamlines is evaluated in appendix C as

$$\frac{F_n}{q}=-\sin\beta\tan\alpha\left(2\omega\sin\alpha+\frac{du}{dm}\right)-\frac{q}{r}\sin^2\beta\sin\alpha\tan\alpha$$

The velocity equation for a radial-bladed impeller without prerotation becomes

$$\frac{dq}{dn}=q\left(\frac{\cos^2\beta}{r_c}-\frac{\sin^2\beta}{r}\frac{dr}{dn}-\frac{\sin^2\beta}{r}\sin\alpha\tan\alpha\right)-2\omega\sin\beta\frac{dr}{dn}-\sin\beta\tan\alpha\left(2\omega\sin\alpha+\frac{du}{dm}\right) \tag{7}$$

Variables dependent upon the impeller geometry or upon values obtained from a previous solution are represented by parameters a and b where

$$a=\frac{\cos^2\beta}{r_c}-\frac{\sin^2\beta}{r}\frac{dr}{dn}-\frac{\sin^2\beta}{r}\sin\alpha\tan\alpha$$

and

$$b=2\omega\sin\beta\frac{dr}{dn}+\sin\beta\tan\alpha\left(2\omega\sin\alpha+\frac{du}{dm}\right)$$

Equation (7) becomes

$$\frac{dq}{dn}=aq-b \tag{8}$$

When equation (8) is solved for q,

$$q=e^{\int_0^n a\,dn}\left(q_0-\int_0^n be^{-\int_0^n a\,dn}dn\right) \tag{9}$$

In solving for q, the term du/dm in parameter b is neglected for the initial solution in order to obtain estimated values of du/dm for the succeeding solution.

Blade surface velocity distribution.—If a linear pressure gradient from blade to blade is assumed, the blade surface velocity distribution may be approximated for a finite number of blades by the method given in appendix D.

Continuity equation.—The equation for continuity of flow through the hub-to-shroud passage may be written

$$w=2\pi\int_0^n rf\rho gq\cos\beta\,dn \tag{10}$$

where f is a factor that takes into consideration the area taken up by the blade cross section. The value of the density ρ is determined from the energy equation (equation (3)) and the relations

$$\frac{\rho}{\rho_{t,t}}=\left(\frac{h}{H_t}\right)^{\frac{1}{\gamma-1}}$$

$$\rho=\rho_{t,t}\left\{1+\frac{\gamma-1}{2}\left[\left(\frac{\omega r}{c_t}\right)^2-\left(\frac{q}{c_t}\right)^2\right]-\frac{\omega\lambda}{gJH_t}\right\}^{\frac{1}{\gamma-1}} \tag{11}$$

NUMERICAL EXAMPLE

IMPELLER EXAMPLE

A numerical example has been computed for an 18-blade mixed-flow centrifugal impeller, the performance of which is described in reference 2. The impeller was designed for a constant cross-sectional flow area from inlet to outlet. The blade curvature is such that the intersection of the blade with any circular cylinder having the same center line as the impeller produces a parabola on the developed cylinder surface. Because of adherence to radial blade elements, the blade angle β increases from hub to shroud.

The operating conditions for the impeller were as follows:

Equivalent impeller tip speed, $U/\sqrt{\theta}$, ft/sec	1331
Ratio of specific heats, γ	1.4
Prerotation at inlet	0
Impeller equivalent weight flow, $W\sqrt{\theta}/\delta$, lb/sec	8.743

PROCEDURES FOR NUMERICAL SOLUTION

The meridional plane of the impeller together with the estimated streamlines and resulting normals is shown in figure 1(a). Estimated streamlines are drawn in between the hub and the shroud; equal mass flow is assumed between the annular stream tubes. Lines normal to the streamlines are drawn in along the flow path.

Radius of curvature.—The radius of curvature of the streamline at any point in the meridional plane r_c is obtained from

$$r_c=\frac{[1+(r')^2]^{3/2}}{r''}$$

The slope of each streamline r' at each normal n is plotted against axial distance in order to obtain the change in slope r''.

Numerical integration.—The velocity q is found by numerically integrating equation (9)

$$q=e^{\int_0^n a\,dn}\left(q_0-\int_0^n be^{-\int_0^n a\,dn}dn\right) \tag{9}$$

The velocity q_0 is the estimated velocity at the hub.

When a is plotted against n (fig. 3(a)) where n is the distance along the normal from hub to shroud, the integral $\int_0^n a\,dn$ can be evaluated by the trapezoidal rule. A plot of $be^{-\int_0^n a\,dn}$ against n can then be obtained (fig. 3(b)) and evaluated in a similar manner. As previously stated, the term du/dm in parameter b is neglected in the first solution. The evaluations of these integrals allow the determination of the velocity q at any point n.

The weight flow at any normal may be obtained from equation (10)

$$w=2\pi\int^n rf\rho gq\cos\beta\,dn \tag{10}$$

When a plot of $rf\rho gq\cos\beta$ against n is used (fig. 3(c)), the integral $\int_0^n rf\rho gq\cos\beta\,dn$ can be evaluated by the trapezoidal rule. If the weight flow does not equal the designated weight flow for the passage, a new value of the velocity q_0 is assumed and the solution is repeated.

In order to satisfy continuity for each stream tube, new streamlines are drawn based on the velocities of the preceding solution. Velocity q (fig. 4(a)) and density ρg (fig. 4(b)) are plotted against n. The radii at which the new streamlines cross the normals are obtained as follows: From

$$\Delta n=\frac{r_{n+1}-r_n}{\cos\alpha}$$

and

$$\Delta w=2\pi rf\rho gq\cos\beta\,\Delta n$$

$$r_{n+1}=\sqrt{r_n^2+\frac{\Delta w\cos\alpha}{\pi f\rho gq\cos\beta}}$$

where $\cos\alpha$, f, ρ, q, and $\cos\beta$ are average values between streamlines based on estimated values of r_{n+1}. After the new streamlines are determined, the normals are drawn. The graphical solution is then repeated for succeeding sets of new streamlines until continuity is satisfied.

ACCURACY

The accuracy of a solution depends to a large extent upon the accuracy with which the streamline curvature is determined. Measurement of other geometrical quantities, of course, enters into the accuracy, but their measurement is more precise.

The sudden decrease in flow area (as much as 25 percent at the hub) from a point just ahead of the blades at the inlet to a point just inside the blades distorts the streamline picture. A tedious and detailed solution is necessary for a true picture of the distortion in this region. Also, the assumption that the flow angle is the same as that of the blades at the inlet is questionable. A lengthy analysis at the inlet was therefore considered unjustifiable.

The cross-sectional area for the clearance is approximately 4 percent near the inlet and affects the maximum flow. In the solution, the clearance area was treated as though the blades extended to the shroud because of continuity considerations.

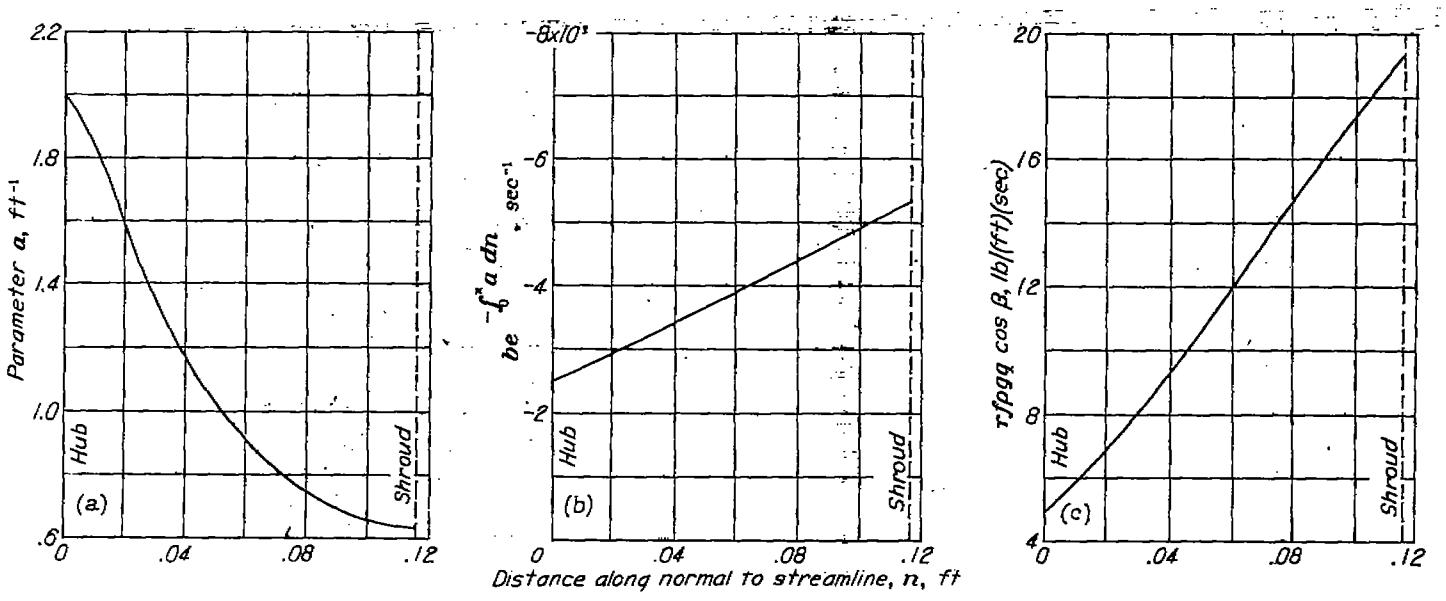

(a) Parameter a.

(b) Exponential $be^{-\int_0^n a\,dn}$

(c) Weight-flow factor.

FIGURE 3.—Plots used for numerical integration of equations (10) and (11).

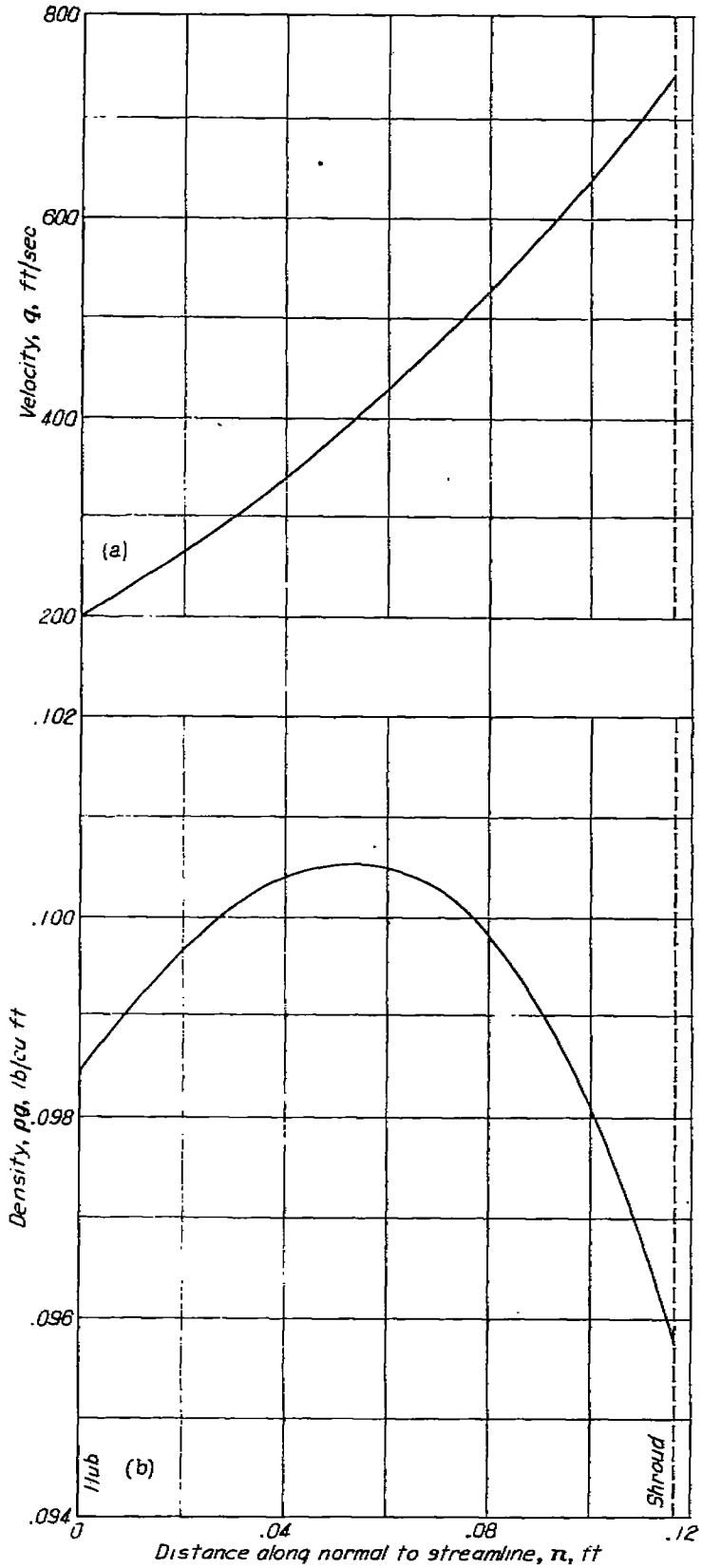

(a) Relative velocity.
(b) Density.

FIGURE 4.—Plots used for computing new streamlines.

RESULTS AND DISCUSSION

A solution of the flow conditions throughout the passage from hub to shroud is shown in figure 5.

Streamlines.—The flow streamlines in the meridional plane are shown in figure 5 (a). Although the solution has been made for equal quantities of flow between streamlines, little information can be derived from the streamline configuration, as shown, other than the direction of flow because the variation in distance between streamlines is due to a variation in blade thickness and radius as well as in velocity. Near the outlet where blade thickness and radius have little effect, however, the streamline spacing indicates considerable variation in velocity across the passage.

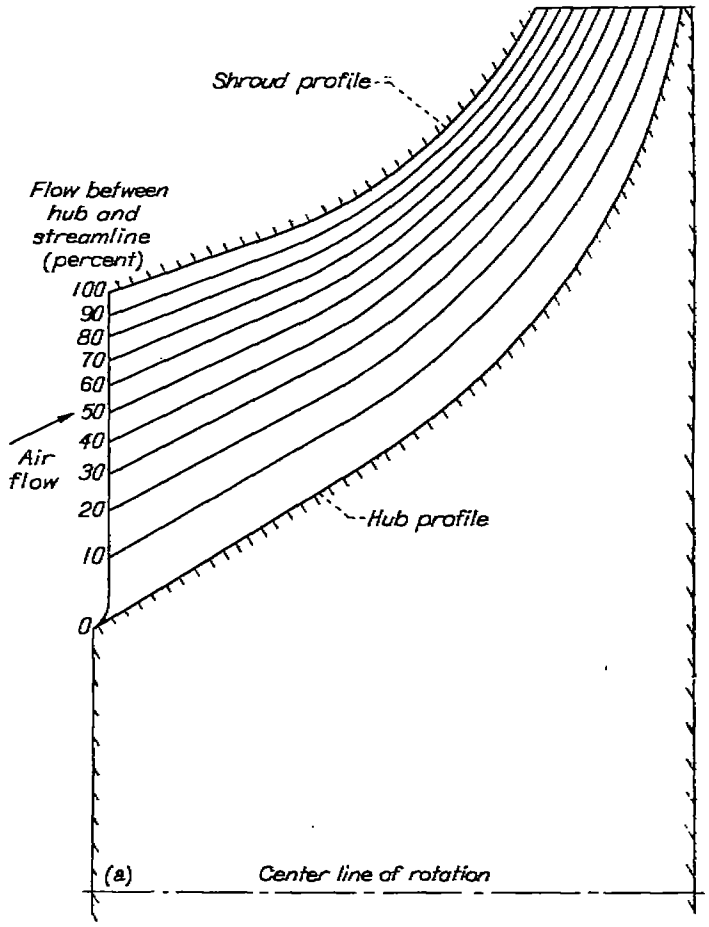

(a) Streamlines for compressible flow.

FIGURE 5.—Flow analysis for centrifugal impeller in meridional plane.

Velocity ratio.—Lines of constant velocity ratio Q relative to the impeller are shown in figure 5 (b). Along the shroud (fig. 6), the velocity is near sonic at the inlet (Mach number, 0.973) with immediate deceleration just inside the impeller and continued deceleration to the outlet, a condition that is highly conducive to boundary-layer build-up and flow separation. A similar condition exists along the straight part of the hub (A to B, fig. 5 (b)). Along the curved part of the hub (B to C), the velocity variation is small with a slight acceleration existing near the impeller outlet.

The relative-velocity distribution as obtained in the solution represents the mean velocity from blade to blade. According to the analysis of reference 1, the velocity along the suction surface is much larger than that along the pressure surface; the velocity varies somewhat uniformly across

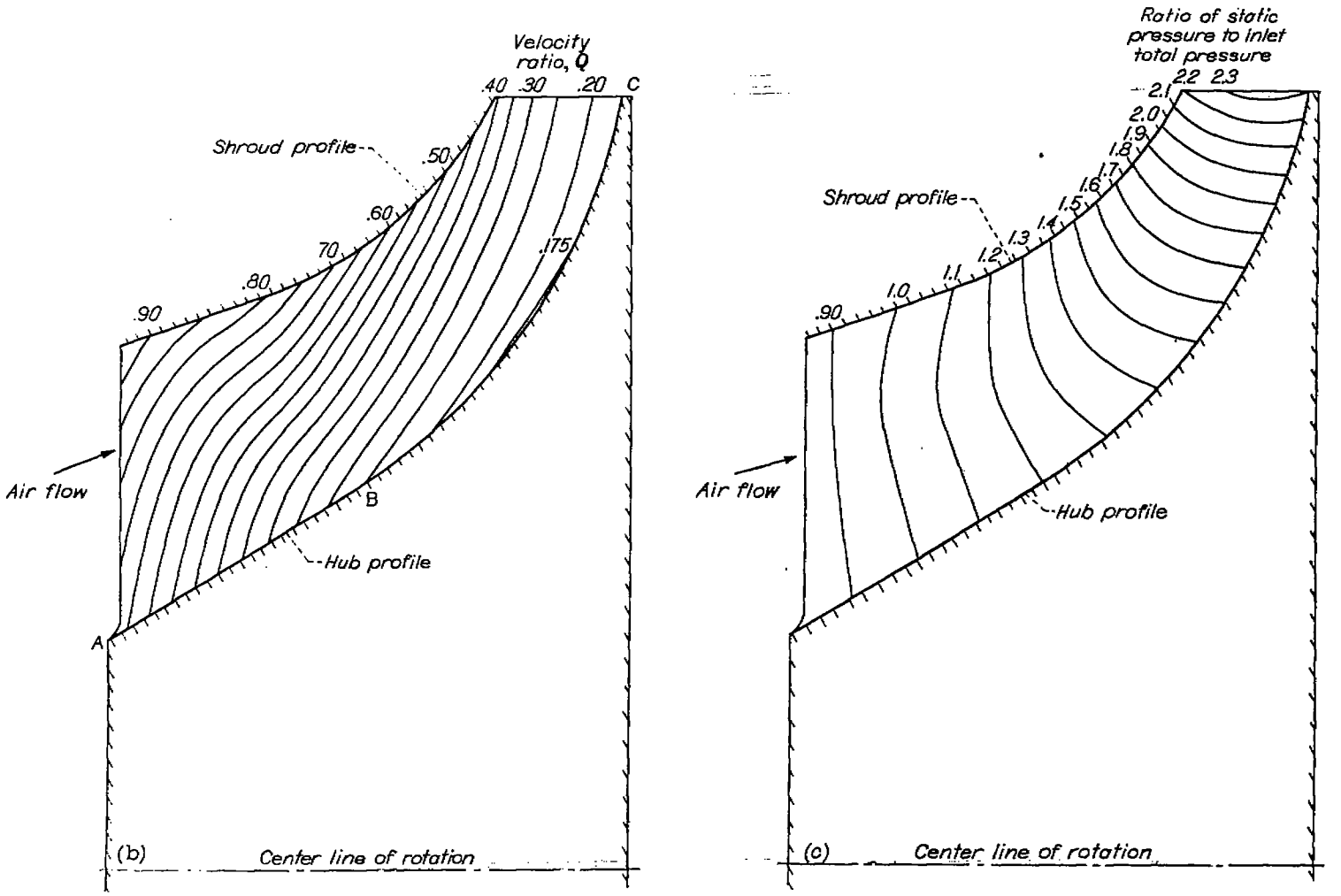

(b) Lines of constant velocity ratio.

(c) Lines of constant pressure ratio.

FIGURE 5.—Concluded. Flow analysis for centrifugal impeller in meridional plane.

the passage. If the blade unloads at the outlet, as it must to satisfy the Kutta condition of tangency at the tip, the decelerations along the suction surface of this blade are of necessity much greater than that shown for the average velocity (fig. 5(b)). Such adverse velocity gradients could easily cause considerable separation along the flow path. At the impeller outlet, these flow separations would result in poor flow conditions with consequent losses at the diffuser inlet.

Pressure ratio.—Lines of constant pressure ratio are shown on figure 5 (c). The pressure lines approximately parallel the normal lines and indicate that static-pressure readings on the stationary shroud of this impeller give representative values for the static pressure across the passage from hub to shroud. In figure 7, experimental values of pressure ratio along the shroud are compared with the theoretical values obtained in the numerical solution. Pressure ratios are shown for the theoretical weight flow and bracketing experimental weight flows. The experimental curve for the higher weight flow represents a point very near the maximum flow or flow cut-off line and shows a large pressure loss near the inlet. The experimental curve for the lower weight flow represents an operating point near maximum efficiency and consequently approaches the theoretical conditions. No pressure drop occurs at the inlet, which is in agreement with the theoretical curve; however, the theoretical pressure increases more rapidly along the shroud because of inefficiency due to friction and flow separation, and because of a velocity increase resulting from flow-area reduction due to boundary layer and from a slightly higher theoretical tip speed.

Maximum flow.—The maximum theoretical weight flow across any normal can be determined by making a series of estimates of velocity at the hub and obtaining the corresponding weight flows. For the numerical example, the greatest restriction of flow occurred just inside the inlet. The maximum flow over a range of tip speeds was determined by the consideration of this flow restriction. Inasmuch as the radius of curvature was infinite for the streamlines near the inlet in the complete numerical solution, it was taken as infinite in computing maximum weight flow at all speeds. A comparison of the theoretical and experimental maximum flow over the speed range is shown in figure 8 (a). The slightly higher theoretical values are in good agreement with the experimental values over a range of tip speeds up to 1400 feet per second (deviation of the order of 3 percent). At speeds above 1400 feet per second, the deviation increased to a maximum value of 7 percent at a tip speed of 1600 feet per second.

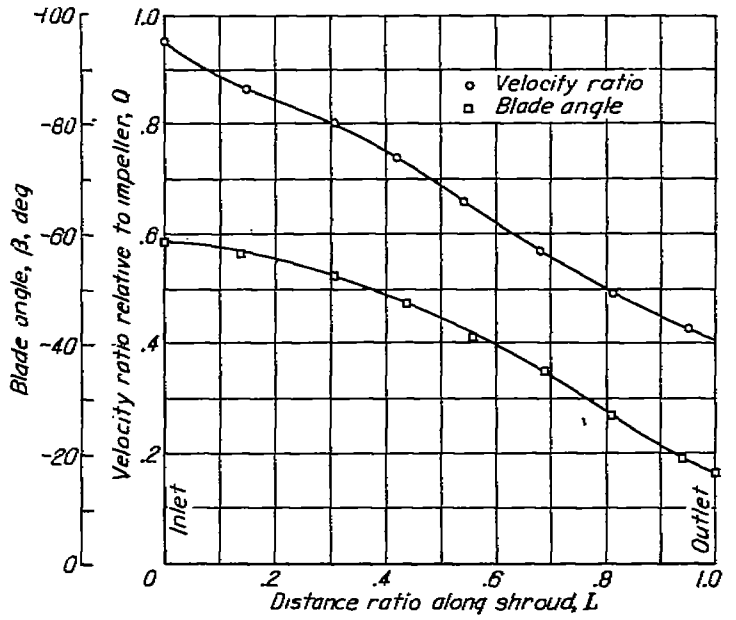

FIGURE 6.—Comparison of relative velocity and blade angle along shroud.

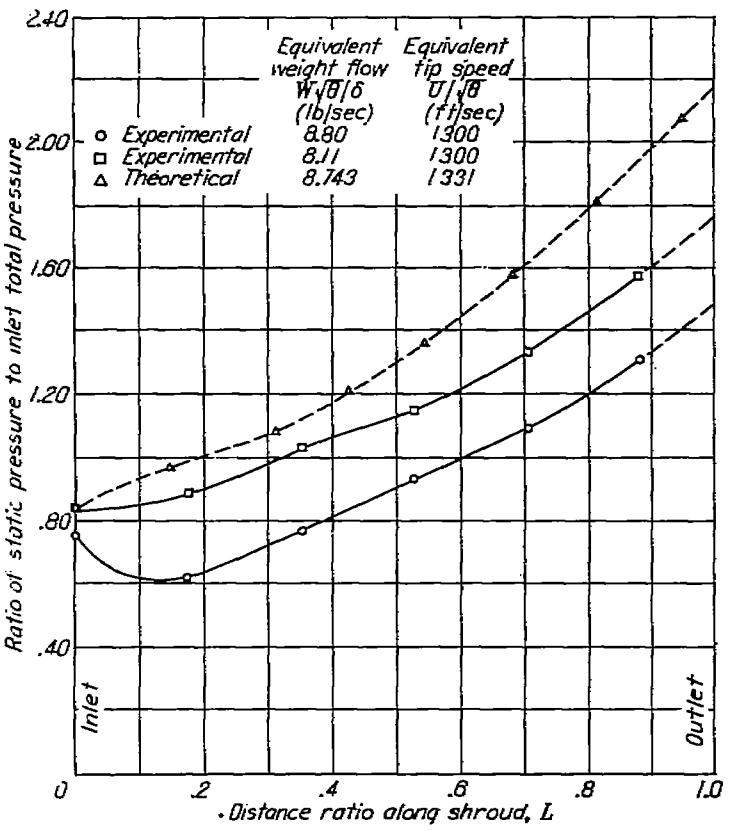

FIGURE 7.—Comparison of theoretical pressure ratio along shroud with experimental values for varying weight flow.

The high relative velocities within the impeller, which caused choking, resulted from the large blade angle β near the impeller inlet. A large inlet blade angle was required for shockless inlet conditions resulting from the consideration of the impeller mass flow and the rotational speed. These high relative velocities, however, can be reduced by an appropriate selection of blade shape to give a more rapid decrease in β near the impeller inlet. A comparison of β

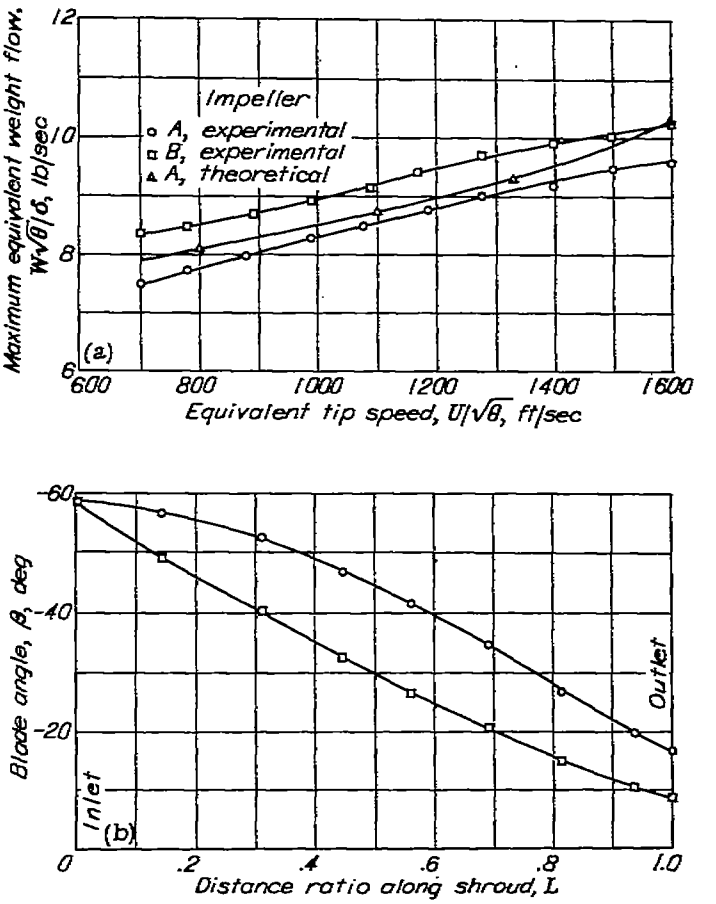

(a) Comparison of maximum flow capacity.
(b) Comparison of blade-angle decrease from inlet to outlet at shroud.

FIGURE 8.—Comparison of change in blade angle and maximum flow capacity of two impellers having same hub-shroud profiles and blade inlet angles.

for the example impeller A and a second impeller B (reference 3) is shown in figure 8(b); β for each impeller is plotted against the distance ratio L along the shroud. Impeller B has the same hub-to-shroud profile and inlet blade angle β as that of the impeller A; however, as indicated in figure 8 (b), the rate of decrease in blade angle for impeller B is much larger near the impeller inlet. The resulting higher flow capacity of impeller B (fig. 8 (a)) may be attributed to the larger rate of decrease of blade angle and consequently lower relative velocities in the impeller passage near the inlet.

SUMMARY OF RESULTS

A method has been developed for a compressible flow analysis between the hub and the shroud of mixed-flow impellers of arbitrary design. Axial symmetry was assumed, but the forces in the meridional plane that are derived from tangential pressure gradients were taken into account. Application of the method to a mixed-flow impeller for which experimental data are available yielded the following results:

1. A large variation in velocity existed across the passage from hub to shroud.

2. Adverse velocity gradients occurred along both hub and shroud surfaces.

3. The theoretical pressure ratio increased more rapidly than the experimental along the shroud from inlet to outlet. Inefficiency of the actual compression process due to flow separation accounts for the greater part of this deviation.

4. The maximum flow over a range of speeds as theoretically determined closely agreed with the experimental.

5. For the example calculation, values of static pressure at any point along the shroud were representative of those across the flow path from hub to shroud.

CONCLUSION

Analysis of flow in the meridional plane of a mixed-flow impeller showed that the rotational forces, the blade curvature, and the hub-shroud profile can introduce adverse velocity gradients along the hub and shroud surfaces.

LEWIS FLIGHT PROPULSION LABORATORY
NATIONAL ADVISORY COMMITTEE FOR AERONAUTICS
CLEVELAND, OHIO, *April 13, 1950*

APPENDIX A

SYMBOLS

The following symbols are used in the calculations and the figures:

a parameter equal to $\frac{\cos^2\beta}{r_c}-\frac{\sin^2\beta}{r}\frac{dr}{dn}-\frac{\sin^2\beta}{r}\sin\alpha\tan\alpha$

b parameter equal to $2\omega\sin\beta\frac{dr}{dn}+\sin\beta\tan\alpha\left(2\omega\sin\alpha+\frac{du}{dm}\right)$

c speed of sound for stagnation conditions, ft/sec

F force per unit mass

f factor accounting for area taken up by blade cross section

g acceleration due to gravity, ft/sec²

H absolute total enthalpy, Btu/lb

h static enthalpy, Btu/lb

J mechanical equivalent of heat

L ratio of distance m at any point to m at impeller exit

m distance along streamline from inlet, ft

N number of blades

n distance along normal to streamline in meridional plane, ft

P total pressure, lb/sq ft

p static pressure, lb/sq ft

Q velocity ratio, q/c_i

q velocity relative to impeller (fig. 1(b)), ft/sec

r radius of particle from axis of impeller rotation, ft

r_c radius of curvature of streamlines in meridional plane (positive in fig. 2(a)), ft

r' slope of streamline in meridional plane with respect to axis of rotation

r'' change in slope r' with respect to axis of rotation

t time, sec

U actual impeller tip speed, ft/sec

u tangential velocity relative to impeller (positive in direction of rotation, fig. 2(c)), ft/sec

v through-flow component of velocity (fig. 2(c)), ft/sec

W total compressor flow rate, lb/sec

w flow rate, lb/sec

z distance in axial direction, ft

α angle between tangent to streamline in meridional plane and axis of rotation, deg

β blade angle (fig. 1, negative for backward-swept blades), deg

γ ratio of specific heats

δ ratio of total pressure at inlet to standard sea-level pressure

θ ratio of inlet stagnation temperature to standard sea-level temperature

λ prerotation term equal to $r_i(\omega r_i+u_i)$

ρ mass density, lb-sec²/ft⁴

ρ_t total mass density, lb-sec²/ft⁴

φ blade angle in axial-tangential direction (negative for backward-swept blades, fig. 2(c)), deg

ω angular velocity of impeller, radians/sec

Subscripts:

a average

d pressure or driving face of blade

i inlet conditions

n indicates position along normal from hub to shroud or normal component

r radial component

s suction or trailing face of blade

z axial component

θ tangential component

0,1 points at succeeding streamlines along normal

APPENDIX B

DEVELOPMENT OF FORCE EQUATION IN HUB-TO-SHROUD PLANE FOR FLOW WHEN AXIAL SYMMETRY IS ASSUMED

Lorenz's equations of motion relative to the rotating impeller, in which axial symmetry is assumed (reference 3), are

$$F_r=\frac{1}{\rho}\frac{\partial p}{\partial r}+\frac{d^2r}{dt^2}-\frac{(\omega r+u)^2}{r}$$

$$F_z=\frac{1}{\rho}\frac{\partial p}{\partial z}+\frac{d^2z}{dt^2}$$

$$F_\theta=\frac{du}{dt}+\frac{u}{r}\frac{dr}{dt}+2\omega\frac{dr}{dt}$$

where the blade force F is the force per unit mass.

From figure 2(a),

$$F_n=F_z\sin\alpha-F_r\cos\alpha$$

where F_n may be evaluated from F_θ (appendix C) as

$$F_n=\frac{1}{\rho}\frac{\partial p}{\partial z}\sin\alpha+\frac{d^2z}{dt^2}\sin\alpha-\frac{1}{\rho}\frac{\partial p}{\partial r}\cos\alpha-\frac{d^2r}{dt^2}\cos\alpha+\frac{(\omega r+u)^2}{r}\cos\alpha \tag{B1}$$

$$\frac{dr}{dt}=v \sin \alpha$$

$$\frac{dz}{dt}=v \cos \alpha$$

$$\frac{d^2r}{dt^2}=v \cos \alpha \frac{d\alpha}{dt}+\sin \alpha \frac{dv}{dt} \tag{B1a}$$

$$\frac{d^2z}{dt^2}=-v \sin \alpha \frac{d\alpha}{dt}+\cos \alpha \frac{dv}{dt} \tag{B1b}$$

$$\frac{dp}{dn}=\frac{\partial p}{\partial z}\frac{dz}{dn}+\frac{\partial p}{\partial r}\frac{dr}{dn}=-\frac{\partial p}{\partial z}\sin \alpha+\frac{\partial p}{\partial r}\cos \alpha \tag{B1c}$$

Substituting equations (B1a) to (B1c) in equation (B1) gives

$$F_n=-\frac{1}{\rho}\frac{dp}{dn}-v\frac{d\alpha}{dt}+\frac{(\omega r+u)^2}{r}\cos \alpha \tag{B2}$$

From figure 2(a),

$$d\alpha=\frac{v\,dt}{r_c}$$

Equation (B2) therefore reduces to

$$\frac{1}{\rho}\frac{dp}{dn}=-\frac{v^2}{r_c}+\frac{(\omega r+u)^2}{r}\frac{dr}{dn}-F_n \tag{B3}$$

APPENDIX C

PROCEDURE FOR EVALUATING BLADE FORCE F_n FOR IMPELLER OF ARBITRARY BLADE SHAPE HAVING RADIAL BLADE ELEMENTS

For an impeller with radial blade elements, a true picture of the blade curvature lies on a circular cylinder having the same center line as the impeller. The blade force F normal to the blade (fig. 2(b)) has the component F_θ, which may be determined from time rate of change of angular momentum in the direction of rotation. The component F_θ as given in appendix B makes the angle φ with the force F.

From figure 2(c),

$$F_n=-F_\theta \tan \varphi \sin \alpha$$

and

$$\tan \varphi=\frac{u}{v \cos \alpha}=\frac{\tan \beta}{\cos \alpha}$$

giving

$$F_n=-F_\theta \tan \beta \tan \alpha$$

From appendix B,

$$F_\theta=\frac{du}{dt}+\frac{u}{r}\frac{dr}{dt}+2\omega\frac{dr}{dt}$$

Substituting $dm=v\,dt$ and $dr/dm=\sin \alpha$ gives

$$F_\theta=v\left(\frac{du}{dm}+\frac{u}{r}\sin \alpha+2\omega \sin \alpha\right)$$

$$F_n=-v \tan \beta \tan \alpha\left(\frac{du}{dm}+\frac{u}{r}\sin \alpha+2\omega \sin \alpha\right)$$

$$F_n=-v \tan \beta \tan \alpha\left(2\omega \sin \alpha+\frac{du}{dm}\right)-\frac{uv}{r}\sin \alpha \tan \alpha \tan \beta$$

From figure 1,

$$v=q \cos \beta$$

$$u=q \sin \beta$$

$$F_n=-q \sin \beta \tan \alpha\left(2\omega \sin \alpha+\frac{du}{dm}\right)-\frac{q^2}{r}\sin^2 \beta \sin \alpha \tan \alpha$$

APPENDIX D

METHOD OF EVALUATING BLADE SURFACE VELOCITIES

From appendix C,

$$F_\theta=v\left(\frac{du}{dm}+\frac{u}{r}\sin \alpha+2\omega \sin \alpha\right)$$

where F_θ is the blade force per unit mass in the tangential direction. Substituting $v=q \cos \beta$, $u=q \sin \beta$, and $dm=\frac{dz}{\cos \alpha}$ gives

$$F_\theta=q \cos \beta\left(\frac{du}{dz}\cos \alpha+\frac{q \sin \beta \sin \alpha}{r}+2\omega \sin \alpha\right) \tag{D1}$$

The quantity $F_\theta\rho$ is the blade force per unit volume, which when multiplied by the circumferential distance between the blades gives the blade force per unit area or the pressure difference between the blades; thus,

$$F_\theta\rho\left(\frac{2\pi rf}{N}\right)=\Delta p \tag{D2}$$

Substituting equation (B1) in equation (B2) gives

$$\Delta p=\rho q \cos \beta\left(\frac{2\pi rf}{N}\right)\left(\frac{du}{dz}\cos \alpha+\frac{q \sin \beta \sin \alpha}{r}+2\omega \sin \alpha\right) \tag{D3}$$

Assuming a linear variation of pressure from blade to blade yields

$$p_s=p_a-\frac{\Delta p}{2}$$

$$p_d=p_a+\frac{\Delta p}{2}$$

Dividing by the total pressure P_i upstream of the impeller inlet gives

$$\frac{p_s}{P_i}=\frac{p_a}{P_i}-\frac{\Delta p}{2P_i} \tag{D4}$$

and

$$\frac{p_d}{P_i}=\frac{p_a}{P_i}+\frac{\Delta p}{2P_i} \tag{D5}$$

Equation (11) is

$$\rho=\rho_{t,i}\left\{1+\frac{\gamma-1}{2}\left[\left(\frac{\omega r}{c_i}\right)^2-\left(\frac{q}{c_i}\right)^2\right]-\frac{\omega\lambda}{gJH_i}\right\}^{\frac{1}{\gamma-1}}$$

For zero prerotation at the inlet ($\lambda=0$) and with

$$\frac{\rho}{\rho_{t,i}}=\left(\frac{p}{P_i}\right)^{\frac{1}{\gamma}}$$

the expression for velocity becomes

$$q^2=(\omega r)^2+\frac{2c_i^2}{\gamma-1}\left[1-\left(\frac{p}{P_i}\right)^{\frac{\gamma-1}{\gamma}}\right] \tag{D6}$$

Substituting equations (B4) and (B5) in equation (B6) gives the final equations for determining the velocity on the blade surfaces,

$$q_s=\sqrt{(\omega r)^2+\frac{2c_i^2}{\gamma-1}\left[1-\left(\frac{p_a}{P_i}-\frac{\Delta p}{2P_i}\right)^{\frac{\gamma-1}{\gamma}}\right]} \tag{D7a}$$

and

$$q_d=\sqrt{(\omega r)^2+\frac{2c_i^2}{\gamma-1}\left[1-\left(\frac{p_a}{P_i}+\frac{\Delta p}{2P_i}\right)^{\frac{\gamma-1}{\gamma}}\right]} \tag{D7b}$$

REFERENCES

1. Stanitz, John D.: Two-Dimensional Compressible Flow in Turbomachines with Conic Flow Surfaces. NACA Rep. 935, 1949. (Supersedes NACA TN 1744.)
2. Anderson, Robert J., Ritter, William K., and Dildine, Dean M.: An Investigation of the Effect of Blade Curvature on Centrifugal-Impeller Performance. NACA TN 1313, 1947.
3. Stodola, A.: Steam and Gas Turbines. Vol. II. McGraw-Hill Book Co., Inc., 1927, pp. 990-997. (Reprinted, Peter Smith (New York), 1945.)